To Engineering Structures

Dynamic Assessment of Shear Connectors in Slab-Girder Bridges

Yong Xia *

School of Civil & Resource Engineering, The University of Western Australia,
Crawley, WA 6009, Australia
Tel: +61-8-6488 2473; Fax: +61-8-6488 1044
xia@civil.uwa.edu.au

Hong Hao
School of Civil & Resource Engineering, The University of Western Australia,
Crawley, WA 6009, Australia
Tel: +61-8-6488 1825; Fax: +61-8-6488 1044
hao@civil.uwa.edu.au

Andrew J. Deeks

School of Civil & Resource Engineering, The University of Western Australia,
Crawley, WA 6009, Australia
Tel: +61-8-6488 3093; Fax: +61-8-6488 1044
deeks@civil.uwa.edu.au

(* Corresponding author)

Total number of pages: 38

Total number of tables: 2

Total number of figures: 15

SUMMARY

Shear connectors are of primary importance in slab-girder bridges to provide composite action. Their damage will reduce the load-carrying capacity of the structure. To test the suitability and efficiency of various vibration-based damage identification methods to assess the integrity of the shear connectors, a 1:3 scaled bridge model was constructed in the laboratory. Some removable anchors were specially designed and fabricated to link the beams and slab that cast separately. Each anchor consists of a threaded bar that penetrates through the soffit of the beam and ties up into an embedded nut cap to simulate a shear connector in the real bridges. Different damage scenarios were introduced by pulling out some connectors. Vibration tests were carried out in each damage scenario. Various damage detection methods have been applied and results show that a local approach was able to detect all the damage successfully and consistently. This new method does not need any reference data for the structure, and therefore it is suitable for application to the prototype bridges. The proposed local method was also compared with some global methods, including optimal model updating technique. Sensitivity region of this local vibration method for damage detection is also investigated.

Key Words: shear connector, slab-girder bridge, damage detection, vibration method

1. BACKGROUND

Shear connectors are widely used in composite bridges that consist of a reinforced-concrete slab supported on steel or concrete girders. They link the slab and the girders together such that part of the slab acts as the flange of the girder resisting longitudinal compression. Shear connectors resist horizontal shear at the girder-deck interface. Damage or failure of the shear connectors will affect the composite action of the bridge girders and slab, and therefore reduce the bridge load-carrying capacity and the horizontal shear resistance.

In Western Australia (WA), about 50 bridges were built in the mid 1970's in the Pilbara region, each based on the same design concepts. The decks of the bridges consist of precast prestressed I-beams supporting a reinforced concrete cast-in-situ slab. Stirrups were embedded in the beams and cast into the slab as shear connectors (or shear links) to connect the beams and slab together. After 30 years in service, the shear connectors may have been damaged, as the region has been flooded a few times, or may not suffice to resist the increasing traffic loadings specified in the new design standard. To investigate the integrity of the bridges, and in particular the shear connectors, the Main Roads Western Australia's (MRWA) bridge No. 986 and No. 852 were chosen for condition assessment through a vibration-based method.

The vibration-based methods have been developed in the past few decades to detect structural damage and/or assess structural condition, because structural properties such as stiffness and damage are closely related to structural vibration parameters, e.g., frequency, mode shape and damping [1]. With regard to the algorithm used, these methods can be classified into direct correlation methods (non-model based) and model updating methods (model-based). The former compares dynamic parameter changes directly while the latter adjusts structural parameters

iteratively. In both categories, the dynamic parameters adopted include frequency response function (FRF) [2], natural frequency [3][4][5], mode shape [6][7][8], mode shape curvature [9], modal flexibility [10][11], and modal strain energy [12][13], and so forth. Via model updating methods [14], the damage can be located and quantified as well by examining the elemental stiffness change [15].

Having been widely and successfully applied to mechanical and aerospace industries, vibration-based methods are gradually being employed on the real civil structures (mainly on bridges). The practical applications to date mainly focus on the model verification or model updating to verify or modify an initial finite element model that is usually based on the design drawings or field observations. The updated model can be used to more reliably predict structural performance under unusual situations such as earthquakes. For example, Brownjohn et al. [16] employed a sensitivity based model updating to improve the correlation of the finite element (FE) model prediction and the field measurements of a curved cable-stayed bridge in Singapore. Recently Zivanovic et al. [17] applied the technique to a footbridge by manual tuning a few critical mechanical parameters. Some researchers have also employed the vibration methods to assess the strengthening effect of the existing structures by measuring the structure vibration properties before and after strengthening. For instance, Zanardo et al. [18] applied shaker and hammer dynamic tests on a flat slab bridge in Australia before and after FRP strengthening. Updated results found that the global stiffness increased by 30%, in a good agreement with the prediction.

However, the real application of vibration methods to structural condition assessment or damage detection is still rare. Researchers from Los Alamos National Laboratory have artificially introduced a number of levels of damage to a highway bridge to be razed and conducted vibration testing before and after each damage increment [19]. Five damage detection algorithms were employed to test their effectiveness and capability. It was found that only the most severe damage

was able to be detected and results were not consistent when applied to the less severe damage. Clearly this kind of study is seldom available in practice. The difficulty of damage detection in real structures lies in that most vibration-based methods require the baseline data (recorded with the structure in an undamaged state) or an accurate FE model, which are usually not available for the existing structures. Another reason is the fact that some features extracted from measurement are not sensitive to the local damage. Moreover, the measurement noise and environmental variation might mask the vibration parameter changes due to damage. As a matter of fact, condition assessment of shear connectors is very rare and limited in literature [20], although static and dynamic analysis of the composite action have been widely studied [21][22].

To detect some possible damage or imperfection in the shear connectors of the two real bridges, effective and reliable methods should be identified. To achieve this, a 1:3 scaled bridge model was built in laboratory to investigate the efficiency of vibration-based damage identification methods. The shear connectors were specially designed not only to simulate failure of particular links, but also to reset them to an undamaged state. The present paper describes the model design and construction, vibration test scheme and discusses the efficiency and reliability of various detection methods. It is found that a local vibration approach comparing the response of the slab and girders directly can detect all the simulated damage scenarios successfully and consistently. The primary advantage of the proposed local vibration approach is that it does not need any reference data for the structure, and it is not sensitive to the changing environment conditions.

2. DESCRIPTION OF THE MODEL

2.1 Model Design

The prototype bridges are briefly described here to allow the context of this laboratory study to be understood easily. The two bridges are continuous four-span and three-span structures, respectively,

which locate in the North West Coastal Highway, in the region of Pilbara WA. The cast-in-situ concrete slab is supported by 7 precast prestressed I-beams. All the beams are connected at the ends by RC diaphragm beams. The diaphragms are in turn seated on elastomeric bearings placed on RC cap beams over piers and abutments. The shear connectors are 12mm in diameter and penetrate the RC slab 100mm before being bent for anchorage. Spacing of the connectors varies from 76 mm in the beam ends to 381mm in the centre of the beams. Figure 1 shows a cross section of a beam and a pair of shear connectors.

The scope of the study is to assess the testing and analysis methods for reliability and practicality, with emphasis on the condition of the shear connectors. The load-carrying capacity is not of concern when designing the model. Therefore the model is not a precise geometrical, structural and material replica of the existing bridges. For example, number of spans, number of girders, material strength and prestressed condition affect the structural capacity but not affect the damage detection methods. Consequently several simplifying assumptions were made as follows:

- the model was reduced to a single span and three girders;
- the model girders were reinforced concrete and not prestressed;
- reinforcement to the girders and slab was scaled;
- the spacing of the model's shear connectors was uniform as opposed to the varied spacing on the actual bridges;
- the number and diameter of the model's shear connectors was modelled such that the relative inertia of the connectors to the girder were similar to that in the real bridges.

The available laboratory space and practical construction considerations led to geometric scaling of approximately one third. Applying geometric scaling resulted in a span 6000 mm in length, beams 100 mm wide by 300 mm deep, diaphragms 210mm × 300mm, and a slab of 50 mm depth, with 475 mm spacing between beams. Figure 2 shows the diagram of the model and details of the shear

connectors. As there are 81 shear connectors in each beam of the prototype, clusters of connectors are combined together and each cluster represented by a single anchor. This resulted in nine connectors at 600 mm intervals along each girder and 8 mm in diameter. The connectors are denoted as S1~S27 in Figure 2.

Design of the shear links incorporates the ability not only to simulate failure of particular links, but also to reset them to an undamaged state. All shear link fixity is provided by securing both ends of the shear link thread. The top end is secured by a T-nut. This is positioned at the mid depth of the slab, and provides anchorage once the slab has been poured. Anchorage between the T-nut and the slab has been achieved by welding a small horizontal metal bar (ϕ6 mm) on top of the T-nut. After the slab pour the T-nut position is permanently fixed. In the lower part, the thread is surrounded by a metal tube which is fixed in place as a result of pouring the concrete beams. To set the shear link to an undamaged state, the thread is screwed into the T-nut, a nut and washer are then positioned and tightened at the beam soffit. To set the link to a damaged state the thread is simply unscrewed from the T-nut and completely removed.

2.2 Model Construction

The model was set up in the Structures Laboratory at the School of Civil and Resource Engineering, the University of Western Australia (UWA). The construction process began with formwork construction and then laying of rebar. The girders and diaphragms rested on two steel frames, which acted as the abutments of the bridge and were fixed to the strong floor. Further description of the model can be found in [23].

The reinforcement scaling in the girders required 2ϕ12 tension reinforcement, 2ϕ12 compression reinforcement and ϕ6-200 stirrups. Two additional pedestals were placed in the middle of the structure and served as temporary support to reduce the downward deflection of the beams during

the curing period. These were removed before testing. Four horizontal stiffeners were also placed at the sides of the beams to reduce the horizontal deformation of the formwork. The first pour was carried out to construct the beams. The second pour to construct the slab took place one week later. After the first pour, the structure was sealed with plastic sheeting during the curing process.

Scaling of the slab to a very thin 50mm depth demanded a smaller concrete aggregate size than usual. Consequently maximum aggregate size of 10mm was adopted in the slab construction. Reinforcement in the slab was chosen as 6 mm in diameter at spacing of 100 mm. The model was left for a period of 28 days before testing commenced in order to ensure that the specified concrete strength was achieved.

3. VIBRATION TESTING

Vibration tests were conducted in this study to detect the removal (‘damage’) of shear connectors in the bridge by investigating changes of the vibration properties such as frequencies, mode shapes, damping ratios and frequency response functions (FRFs).

The aim of building the model was to find an effective scheme of vibration testing to be applied to the prototype structures. The intact state and several damage states (simulated by loosening the connectors) were tested using hammer impact. Four damage scenarios (denoted as D1 to D4) are investigated here, together with the intact state (D0). For D1, the anchors S13 and S14 (referring to Figure 2) were removed from the girder, for D2 S4 and S5 were taken out, and for D3, in addition to S4 and S5, S8 and S9 were also removed. In damage scenario D4, only S15 was taken out. This damage scenario was used to determine the sensitivity radius of local vibration method for detection of damage in shear connectors. The connectors in different places and different beams were

removed to verify the effectiveness and reliability of the methods in dealing with different damage scenarios. In each case the measurement points are presented in Table 1.

In each case accelerometers were placed on the slab (denoted as “SA”, “SB” and “SC”) and/or underneath the girders (denoted as “GA”, “GB” and “GC”) as shown in Figure 3. Twelve sensors were used. Four impact tests were performed in each set to average the data. For each impact 4096 points of data were recorded with a sampling frequency of 500 Hz, which resulted in 2049 frequency lines from 0 to 250 Hz. Vertical response was measured in all cases. The vibration properties such as frequencies, mode shapes and damping were extracted from the FRFs by the Rational Fraction Polynomial method [24].

4. DAMAGE IDENTIFICATION WITH GLOBAL METHODS

Here global methods denote damage detection using global vibration properties such as frequencies and mode shapes extracted from the measurements on the slab. Most of the current vibration-based damage detection exercises in the literature use modal data recorded before and after the onset of damage.

4.1 Global Modal Data

Table 2 compares the natural frequencies, damping ratios and modal assurance criterion (MAC) of mode shapes between the undamaged state D0 and the damaged state D1. From Table 2, it can be seen that frequency differences between the states are insignificant until mode 13. Actually frequency change below 0.5% is of similar level to the measurement noise [25]. Due to length limitations, comparison for other damage cases is not shown here. However, it was found that for states D2 and D3 frequency differences from the undamaged state are not significant until mode 13 and mode 7, respectively, and the differences in D3 are more significant as the damage is more

severe. Regarding the mode shapes, the situation is quite similar, in which only the higher modes display noticeable changes. Damping ratios generally increase slightly in the damaged states. Due to the difficulty of measuring it accurately, damping is rarely used in damage detection. These observations indicate that global method may not be a good approach for shear connector damage identification, since vibration properties of high modes are difficult to measure accurately in practice.

4.2 Direct Comparison

Two direct methods are used here to detect damage. One is to examine the Coordinate Modal Assurance Criteria (COMAC) [24] between the mode shapes of the girder (ϕ_G) and the corresponding slab points (ϕ_S). For point q, the COMAC is defined as

$$COMAC(\phi_G, \phi_S, q) = \frac{\left(\sum_{i=1} \left| (\phi_i^q)_G (\phi_i^q)_S \right| \right)^2}{\left(\sum (\phi_i^q)_G{}^2 \right) \left(\sum (\phi_i^q)_S{}^2 \right)} \quad (1)$$

Here ϕ_i^q is the i-th mode shape value at point q. Usually a bad correlation of mode shapes results in a low COMAC value, which indicates possible damage around the point.

Figure 4 shows the COMAC of the damaged state D1 and the undamaged state D0 with respect to the measurement points (SA1~12, SB1~12 and SC1~12). As shown, COMAC values at the points SB5~SB7 are small, indicating the damage present in the area. However, COMAC values at some other locations are also small, for example, points SC4~SC6 and the supports, where damage is not present. The small values near the supports are due to the fact that the modal deflections are close to zero at these points, and thus small perturbation (for example, measurement noise) will cause a large decrease of correlation. This observation indicates possible false identification if this approach is used.

Another method is to examine the flexibility change. The flexibility matrix can be estimated from the measured modal frequencies and mass-normalized mode shapes [10][11]:

$$[F] = \sum_{i=1}^{n} \omega_i^{-2} \{\phi_i\}\{\phi_i\}^T \quad (2)$$

where ω_i is the i-th circular frequency. Figure 5 shows the flexibility changes between D0 and D1. For clarity, the diagonal values in the flexibility matrix are plotted with respect to the measurement points. In the figure, the largest flexibility increase is located at SB6, and therefore the damage is correctly detected. Again, there is some false identification of damage at points SC4~SC9, which may be due to the damage in S13 and S14 affecting the mode shapes in these locations. Points SA2~SA10 show flexibility decrease in the damaged state, implying stiffness increase in this area. This might be caused by measurement error or because some modes were not well excited.

4.3 Model Updating

An FE model, as illustrated in Figure 6 was built to detect the artificial damage via a two-stage model updating technique [15]. In the present study, a connector is modelled as a short beam element which links the slab and girders. The upper node of a connector coincides with the central axis of the slab which is modelled as shell elements, and lower node of a connector coincides with the upper joint of the corresponding girder which is also modelled as shell elements. The mesh is finer around S15 in order to study the sensitivity region for damage detection (discussed later). Details of the model are presented in reference [27]. The FE model was first constructed in ANSYS [29]. Its geometry and element information were then passed into a MATLAB [26] based software package for modal analysis and model updating. An initial model (IM) was formed based on the measured geometry of the structure and the material parameters obtained through testing of three specimens. The IM was updated so that the analytical frequencies and mode shapes matched those measured in the undamaged state (D0). The updated model in D0 is referred as UM to represent the undamaged structure. Then the UM was updated again to match the measured frequencies and

mode shapes in the damaged state. The new model DM represents the damaged state of the structure. Comparing the elemental parameters of UM and DM, the damage can be identified.

With the Optimisation Toolbox in MATLAB, element stiffness of all members of the structure in the intact state and damaged states were identified. Figure 7 shows the damage indicator (DI) of the shear connectors in the damaged state D3. In the present study, DI is defined as the ratio of the bending stiffness change in the updated damage model (DM) to that in the undamaged model (UM). The white bars denote negative values while the grey ones indicate positive values. It can be seen that at the locations with removed connectors (S4, S5, S8 and S9), there are large negative DI values. It is noted that these larger DI values extend to a few healthy elements nearby, and there are some positive DIs, which might be due to the error in the measurements or a nonlinear effect that has been observed by many other researchers. Nevertheless, the damage location was successfully detected.

5. DAMAGE IDENTIFICATION WITH LOCAL METHODS

In the above methods, both undamaged and damaged data are required. For most bridges, the undamaged data can only be obtained from an FE model based on design drawings, which may result in errors in representing the true bridge vibration properties. To overcome this, a new local approach is proposed here. This method is based on the fact that when the connectors are removed, the slab separates from the beam, and the nearby points may respond differently from those on the beam. To achieve this, sensors were placed on top of the slab to measure response of the slab, and also underneath the corresponding girder to record its response. Directly comparing the measured responses of the slab and girders was anticipated to allow detection of the ‘damage’ of the shear connecters.

5.1 Vertical Response

Two DIs are used to evaluate the condition of the shear connectors. The first one is the correlation of the vertical FRFs (COFRF) of the girder and the corresponding slab points, in a procedure resembling the COMAC technique:

$$COFRF\left(H_i^G, H_i^S\right) = \left\| \left\{H_i^G\right\}^T \left\{H_i^S\right\} \right\|^2 \Big/ \left(\left\| \left\{H_i^G\right\} \right\| \cdot \left\| \left\{H_i^S\right\} \right\| \right)^2 \tag{3}$$

Another indicator is the relative difference of the FRFs (RDFRF) between the girder and the slab, which is defined as

$$RDFRF\left(H_i^G, H_i^S\right) = \left\| \left\{H_i^G\right\} - \left\{H_i^S\right\} \right\| \Big/ \left\| \left\{H_i^G\right\} + \left\{H_i^S\right\} \right\| \tag{4}$$

where H_i is the FRF measured at the i^{th} point, superscripts "G" and "S" represent girder and slab, respectively, $\|\cdot\|$ denotes the Euclidean norm, and $\{\}$ is the vector of FRF including all measured frequency lines. A high COFRF and/or a low RDFRF value means a high correlation of the response of the point on the slab with the corresponding point on the girder. On the other hand, a low COFRF and/or a high RDFRF value means a significant difference in the responses at the particular point, which indicates damage in the vicinity.

Figure 8 ~ Figure 11 show the results of the two damage indicators calculated for damage states D0~D3. In Figure 8, COFRF and RDFRF of D0 are plotted in terms of 36 measured points. This figure shows that all COFRF values are larger than 0.93 and all RDFRF are less than 0.17 in the undamaged state, indicating that the FRFs on the slab are quite close to those underneath the girders. In the damaged state D1, the indicators at SA1~12 and SC1~12 do not show noticeable changes compared with D0. As shown, at point SB6 (the damaged location) the RDFRF decreases to 0.75 and the COFRF increases to 0.36, while the indicators away from SB6 remain essentially unchanged with high COFRF and low RDFRF. This indicates that the damage is detected successfully and no false identification has occurred. For the damage state D2, where simulated

damage is in Girder A, only the points on the slab and GA1~12 were measured (see Table 1). SA6 shows a low COFRF and high RDFRF values. For the multiple damage state D3, the two damage locations (SA6 and SA10) are also clearly identified. Therefore, with this local approach, all the damage has been located successfully without false identification. The results are consistent and the method is robust. It must be noted that the two indicators are calculated by comparing the FRFs on the slab and those underneath the girder point by point over the whole frequency range (0~250 Hz here), within the same undamaged or damaged state. Consequently the indicators in each state can be evaluated individually and the intact data is not necessary (DIs calculated for the undamaged state D0 are just presented here for comparison).

5.2 Horizontal Response

The horizontal responses of GA1~GA12 and SA1~SA12 were also recorded in damage states D0 and D3. Using the same formula as (3) and (4), the two indicators are calculated. The results are not shown here for brevity. It has been found that even with no damage present the RDFRF values are quite large, while the presence of damage causes only insignificant change. This is because the connector's rigidity in the horizontal direction (shear) is not as strong as that in the vertical (axial) direction. Similar results have been found in Reference [20]. Consequently vertical RDFRF values in the undamaged state are smaller than the horizontal ones, and damage detection using vertical responses is more reliable. Therefore, it is concluded that horizontal vibration measurement is not a good choice for damage detection of shear connectors between bridge slab and girders using the proposed local vibration method.

5.3 Sensitivity radius of local vibration method for damage detection

From the figures presented above it is clear that the damage of connectors only affects the measured vibration data near these connectors. For example in D2, removing S4 and S5 leads to a significant change in SA6 (middle of S4 and S5), minor changes in SA5 and SA7, and almost no change in

vibration data measured in other sensors. Therefore, it is important to determine the sensitivity radius of shear connector damage for the vibration data so that an appropriate testing scheme can be designed for prototype bridges. To achieve this, vibrations at points around connector S15 were measured before and after removal of the connector (damage state D4). Nine sensors were placed on the slab near the damage (SB13~SB21) and at corresponding points on the beam (GB13~GB21). The distances between these points and S15 are 25, 100, 150, 200, 300 and 400 mm, as shown in Figure 12.

Using the approach described above, the FRFs of the nine points are obtained and the RDFRF is shown in Figure 13 for the undamaged (D0) and damaged (D4) cases. It can be seen that in D0 the difference is always less than 0.1. In D4, the maximum difference occurs at points near S15 and the difference decreases as the distance increases. At points 300mm away, RDFRF are about 0.2, while at points 400 mm away the difference is only about 0.1 only. Therefore the reliable damage detection range is about 300 mm. This implies that damage in a connector can cause significant change in vibration properties at points within a 300 mm radius. This conclusion is also supported by observation of Figure 9 ~ Figure 11. When the sensors are placed in this range, the damage can be reliably detected, otherwise it cannot be reliably identified. Consequently distance between the sensors should be 600 mm to detect possible damage in all the connectors. Obviously this detectable range depends on the structure. For the prototype bridges, the sensitivity radius is not necessarily 300 mm or 900 mm (300 by the scale factor of 3). To find the sensitivity radius on a real bridge, a numerical study can be carried out through a FE analysis. As an example, the current model structure is employed here.

The fine mesh around S15 is shown in Figure 14. The slab and girders are modelled by shell elements and there is no connection between them except the shear connectors modelled by beam elements. In the damaged case, the link element at S15 is removed. The FRFs of 16 points around

S15 on the slab and those underneath the beam are directly compared, as was done for the experimental results. The various distances to S15 are 0, 25, 100, 150, 200, 250, 300, 400, 500 and 600 mm. Here FRFs are synthesized from the analytical frequencies, mode shapes and damping through the equation [24]:

$$H_{jk}(\omega) = \sum_{r=1}^{N} \frac{\phi_{jr}\phi_{kr}}{\omega_r^2 - \omega^2 + 2i\omega\omega_r\xi_r} \tag{5}$$

where H_{jk} is the FRF of point j due to the input excitation at point k at circular frequency ω, ϕ_{jr} and ϕ_{kr} are the r^{th} mode shape values at point j and k, ω_r is the r^{th} circular frequency and ξ_r the r^{th} damping ratio, N is the number of modes in the frequency band of interest (0~250 Hz here) and $i=\sqrt{-1}$. It is noted that the frequencies and mode shapes are obtained from the FE model, while the damping ratios are taken from the measurements, as the initial FE model is undamped.

The RDFRF of the 16 points in the undamaged state and damaged state (removing S15) are compared in Figure 15. In the intact state, the maximum difference of the FRFs is less than 5%. In the damaged structure, the maximum difference occurs in the damage location and the difference decreases as the distance of points to S15 increases, as expected. For the point with a distance of 400 mm, the RDFRF is about 9%, still significantly larger than the undamaged ones. For the point with a distance of 500 mm, the RDFRF decreases to less than 5% and the change is not discernable. Therefore, the detectable damage radius is indicated to be 400 mm, which is a little larger than the experimental result. Since there is some degree of noise in testing, the experimental result (300 mm) is reasonable.

6. CONCLUSIONS AND DISCUSSIONS

This study is the first attempt to detect possible damage of shear connectors in slab-girder bridges through vibration methods. A 1:3 scaled RC bridge model was built in the laboratory to investigate the suitability of vibration-based methods for detecting possible damage of shear connectors between bridge girders and slab. Removable anchors were used to simulate the shear connectors of the real bridge. Simulation of shear connector damage at different locations was achieved by pulling out some of the connectors. Vibration testing was carried out before and after each damage case. Based on the results achieved with the global and local approaches, the following conclusions are drawn:

1. From the global vibration data (frequencies and mode shapes), damage locations can be identified via an optimisation-based model updating technique when both undamaged and damaged data were available. COMAC and flexibility methods can detect some damage location but also make some false identification.
2. Local vibration data, in particular the vertical responses of the girders and slab, were compared directly and could be used to identify damage in shear connectors accurately and consistently.
3. In the local approach, reference data from the undamaged state is not necessary, and thus the technique is suitable for identifying damage in shear connectors in existing bridges.

The sensitivity radius for damage detection was also studied. It was found that if sensors were placed less than 300 mm from the damage, the damage can be detected, whereas the damage cannot be detected if the sensors were placed more than 300 mm from the damage. These results were also verified through FE simulation.

The present methods will be applied to the prototype bridges. As many researchers have indicated [25][28], the changing environment especially the temperature affects the frequencies, mode shapes and damping. Consequently it affects condition assessment that is based on the changes in modal data before and after onset of damage. This is because it cannot differentiate between the changes in

the modal data due to the damage or due to the changing environment. However, as the data of the slab and the girders are measured simultaneously in the present local method, the changing environment has similar effect on both sets of data (on the slab and those of the girders). Consequently the environmental effect is minimized.

The local approach is based on the fact that removal of the shear connectors leads to the slab separating from the girders to a certain extent, and so the nearby points on the slab respond differently from those on the girders. The ideal solution is to measure the vibration close to the interface of the slab and girders, that is, measure the response of the bottom of the slab and top of the girders. However, taking into account the need for practical implementation, the sensors were placed on the top of the slab and underneath of the girders in the present study. This may introduce some errors. However, numerical simulation via the FE model found that 50% stiffness loss of the entire slab only increases RDFRF by about 0.01 implying this local method is relatively independent of the slab and girder conditions. Therefore, the error introduced by placing the sensors on top of the slab and underneath of the girder will not be significant.

ACKNOWLEDGEMENTS

This research was performed under the support from a Linkage Project LP0453783 sponsored by Australian Research Council (ARC) and Main Roads Western Australia (MRWA). Special thanks are extended to Robert Scanlon, Adam Lim, Erica Smith, Mark Watkins, Jessica Willis and Kirk Ballantyne. The first author is also grateful to Dr. Xinqun Zhu for his valuable comments.

REFERENCES

[1] Doebling SW, Farrar CR, Prime MB, Shevitz DW. Damage identification and health monitoring of structural and mechanical systems from changes in their vibration characteristics: a literature review. Los Alamos National Laboratory Report LA-13070-MS. 1996.

[2] Rad SZ. Methods for updating numerical models in structural dynamics. Ph.D. Thesis, Imperial College, University of London, 1997.

[3] Cawley P, Adams RD. The locations of defects in structures from measurements of natural frequencies. Journal of Strain Analysis, 1979; **14**: 49–57.

[4] Stubbs N, Osegueda R. Global damage detection in solids – experimental verification. Modal Analysis: The International Journal of Analytical and Experimental Modal Analysis, 1990; **5**: 81–97.

[5] Hearn G, Testa RG. Modal analysis for damage detection in structures. Journal of Structural Engineering, ASCE, 1991; **117**: 3042–3063.

[6] Kam TY, Lee TY. Detection of cracks in structures using modal test data. Engineering Fracture Mechanics, 1992; **42**: 381–387.

[7] Kaouk M, Zimmerman DC. Structural damage assessment using a generalized minimum rank perturbation theory. AIAA Journal, 1994; **32**: 836–842.

[8] Ricles JM, Kosmatka JB. Damage detection in elastic structures using vibratory residual forces and weighted sensitivity. AIAA Journal, 1992; **30**: 2310–2316.

[9] Pandey AK, Biswas M, Samman MM. Damage detection from changes in curvature mode shapes. Journal of Sound and Vibration, 1991; **145**: 321–332.

[10] Pandey AK, Biswas M. Damage detection in structures using changes in flexibility. Journal of Sound and Vibration, 1994; **169**: 3–17.

[11] Aktan AE, Lee KL, Chuntavan C, Aksel T. Modal testing for structural identification and condition assessment of constructed facilities. Proceedings of 12th International Modal Analysis Conference, 1994; 462–468.

[12] Dong C, Zhang PQ, Feng WQ, Huang TC. The sensitivity study of the modal parameters of a cracked beam. Proceedings of the 12th International Modal Analysis Conference, 1994: 98–104.

[13] Shi ZY, Law SS, Zhang LM. Structural Damage Localization from Modal Strain Energy Change. Journal of Sound and Vibration, 1998; 218(5): 825–844.

[14] Friswell MI, Mottershead JE. Finite Element Model Updating in Structural Dynamics. Dordrecht (The Netherlands): Kluwer Academic Publishers; 1995.

[15] Xia Y, Hao H, Brownjohn JMW, Xia PQ. Damage Identification of Structures with Uncertain Frequency and Mode Shape Data. Earthquake Engineering and Structural Dynamics 2002; 31 (5): 1053-1066.

[16] Brownjohn JMW, Xia PQ, Hao H, Xia Y. Civil Structure Condition Assessment by FE Model Updating: Methodology and Case Studies. Finite Elements in Analysis and Design 2001; 37 (10): 761-775.

[17] Zivanovic S, Pavic A, Reynlods P. Model testing and FE model tuning of a lively footbridge structure. Engineering Structures 2006; 28 (6): 857-868.

[18] Zanardo G, Hao H, Xia Y, Deeks A. Condition Assessment through Modal Analysis of A Run-on RC Slab Bridge Before and After Strengthening. Journal of Bridge Engineering ASCE 2006, accepted.

[19] Farrar CR, Jauregui DV. Damage Detection Algorithms Applied to Experimental and Numerical Modal Data From the I-40 Bridge. Los Alamos National Laboratory report, LA–13074–MS. 1996

[20] Dilena M, Morassi A. Experimental Modal analysis of steel concrete composite beams with partially damaged connection. Journal of Vibration and Control 2004; 10: 897-913.

[21] Sapountzakis EJ, Katsikadelis JT. A New Model for the Analysis of Composite Steel - Concrete Slab and Beam Structures with Deformable Connection. Computational Mechanics 2003; 31(3-4): 340-349.

[22] Sapountzakis EJ. Dynamic Analysis of Composite Steel-Concrete Structures with Deformable Connection. Computers and Structures 2004; 82(9-10): 717-729.

[23] Xia Y, Hao H, Zanardo G, Deeks A. Condition Assessment of Shear Connectors in WA Bridges – Laboratory Study. In: First International Conference on Structural Condition Assessment, Monitoring and Improvement, Perth, Australia, 2005. 357-364.

[24] Ewins DJ. Modal Testing – Theory, Practice and Application. Baldock (Hertfordshire, UK): Research Studies Press Ltd; 2000

[25] Xia Y, Hao H, Zanardo G, Deeks A. Long Term Vibration Monitoring of A RC Slab: Temperature and Humidity Effect. Engineering Structures 2006; 28 (3): 441-452.

[26] MATLAB, 2005, Optimization Toolbox User's Guide, Version 3, The Mathworks, Inc., Natick, USA.

[27] Xia Y, Hao H, Deeks A. Vibration-based Damage Detection of Shear Connectors in Nickol River Bridge and Balla Balla River Bridge, Part II: Laboratory Study. School of Civil &

Resource Engineering, The University of Western Australia, Australia, Report No. ST-05-02. 2005.

[28] Farrar CR, Doebling SW, Cornwell PJ, and Straser EG. Variability of Modal Parameters Measured on the Alamosa Canyon Bridge. Proceedings of the 15th International Modal Analysis Conference, 1997: 257-263.

[29] ANSYS 8.1. ANSYS Inc., Southpointe, PA, USA. 2004.

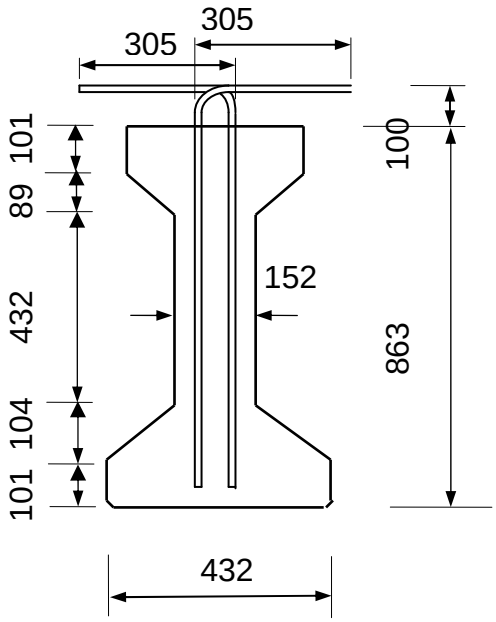

Figure 1. Beam and Shear connectors in the real bridges (unit: mm, not to scale)

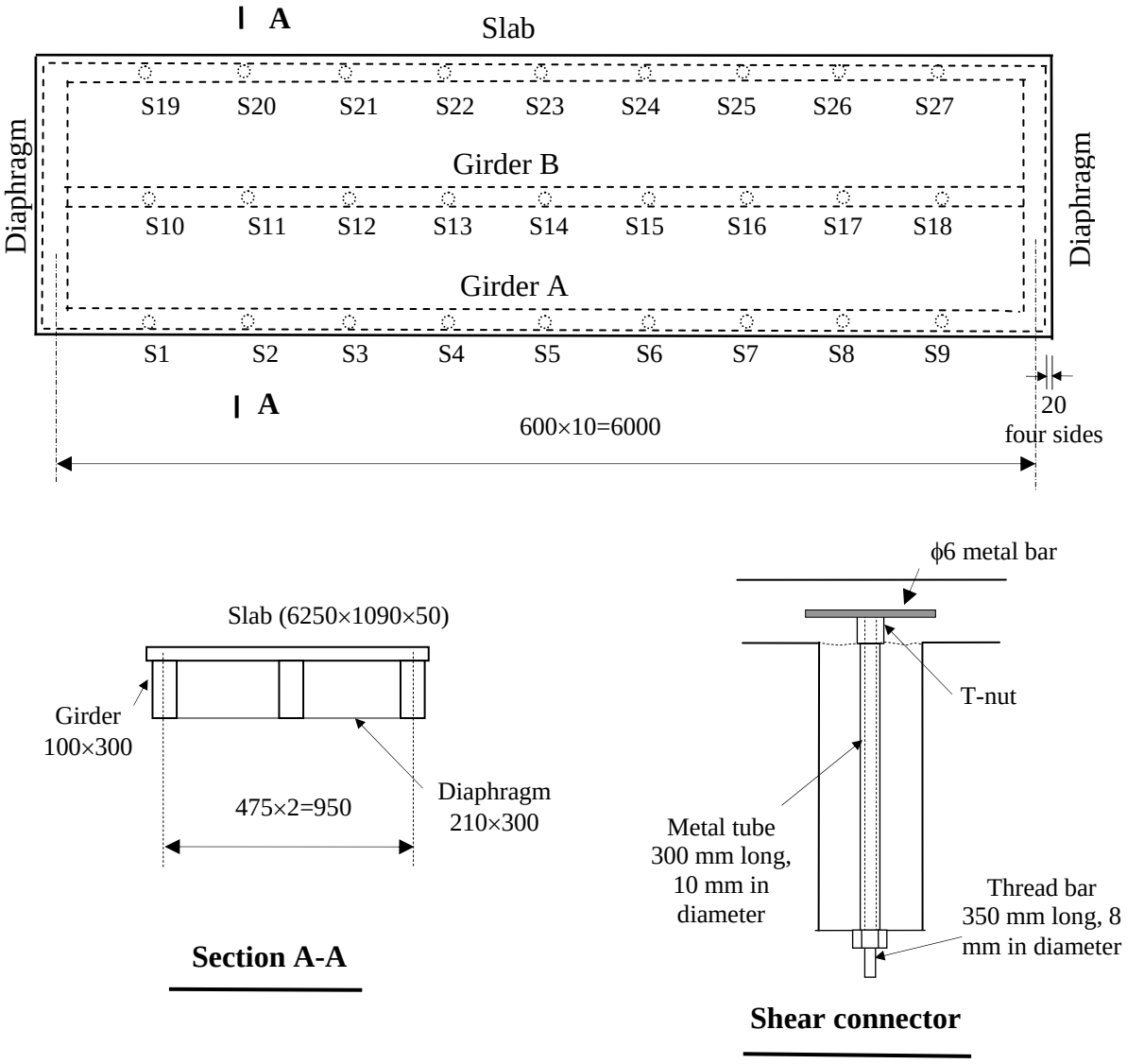

Figure 2. Plan of the model and details (unit: mm)

○ Shear connectors (27 in total)

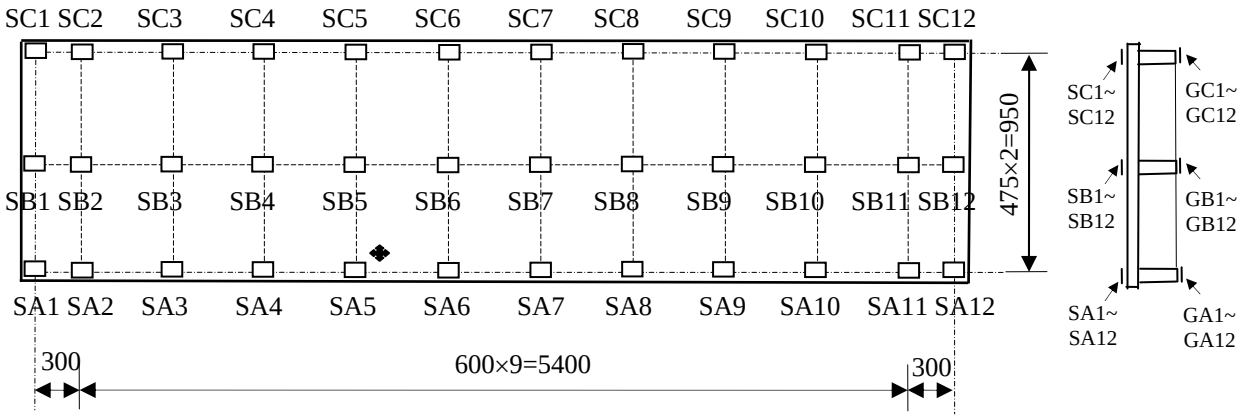

Figure 3. Sensor layout on the slab and underneath the girders

(✥ hammer location, ▭ sensor location)

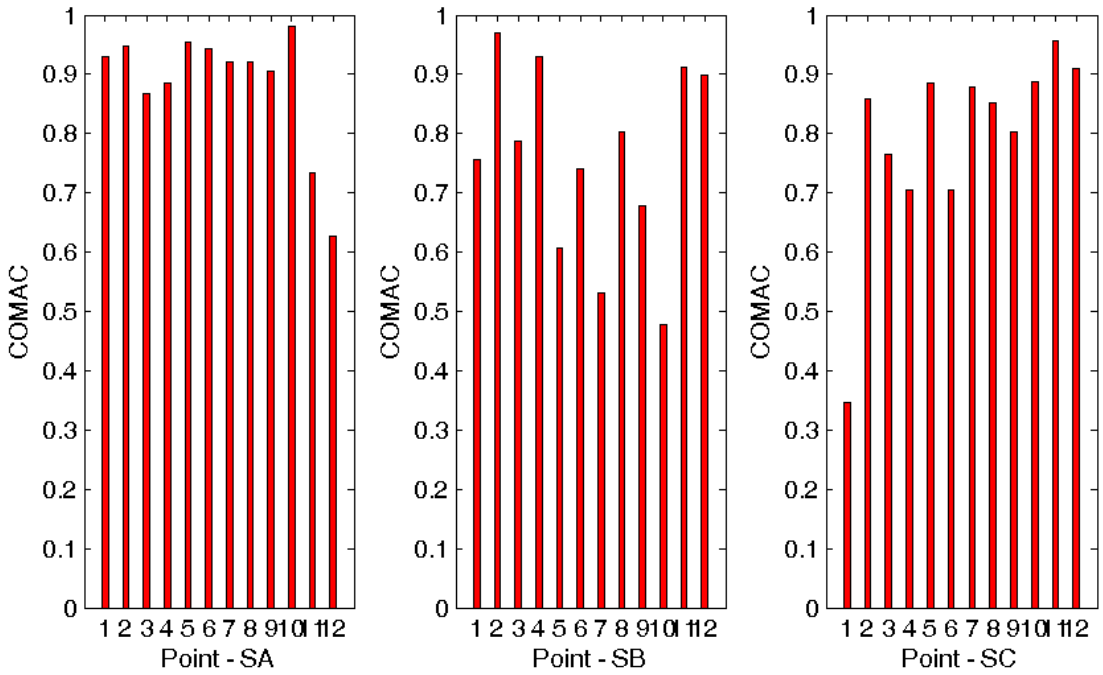

Figure 4. COMAC of D0 and D1 (true damage locates around SB6)

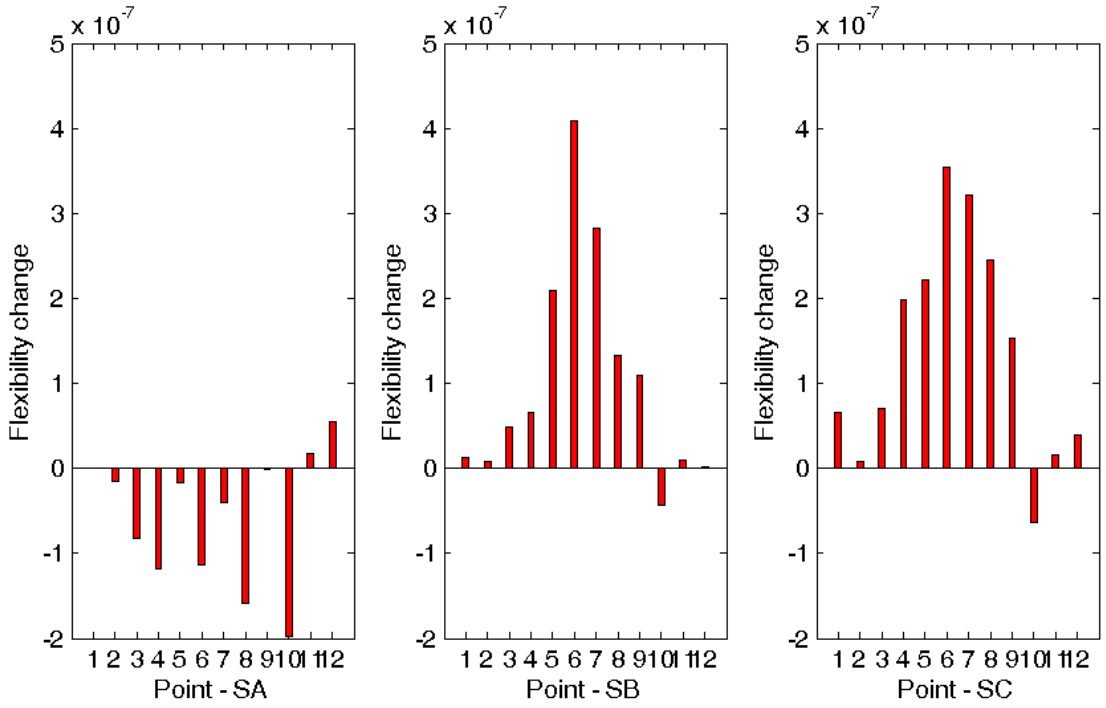

Figure 5. Flexibility change between D0 and D1 (true damage locates around SB6)

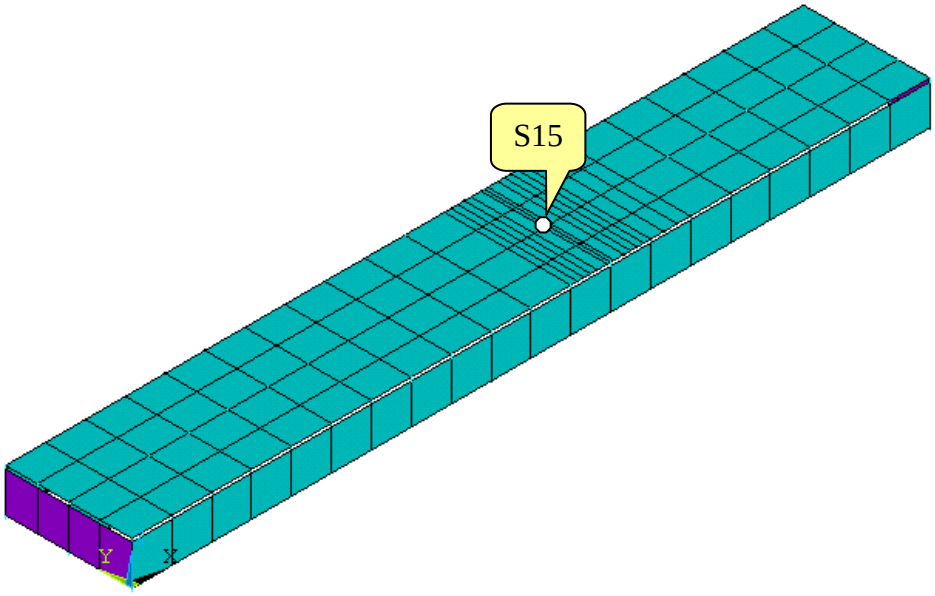

Figure 6. FE model of the structure and location of shear connector S15

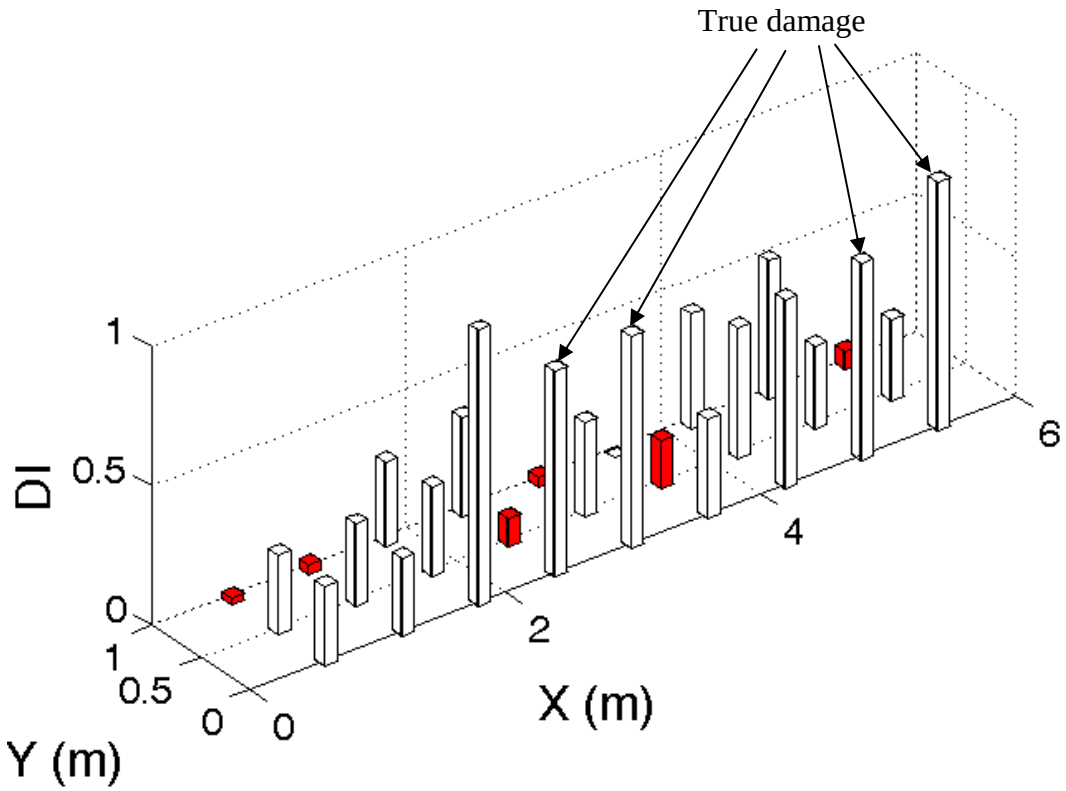

Figure 7. Damage Indicators of case D3 in terms of connector location

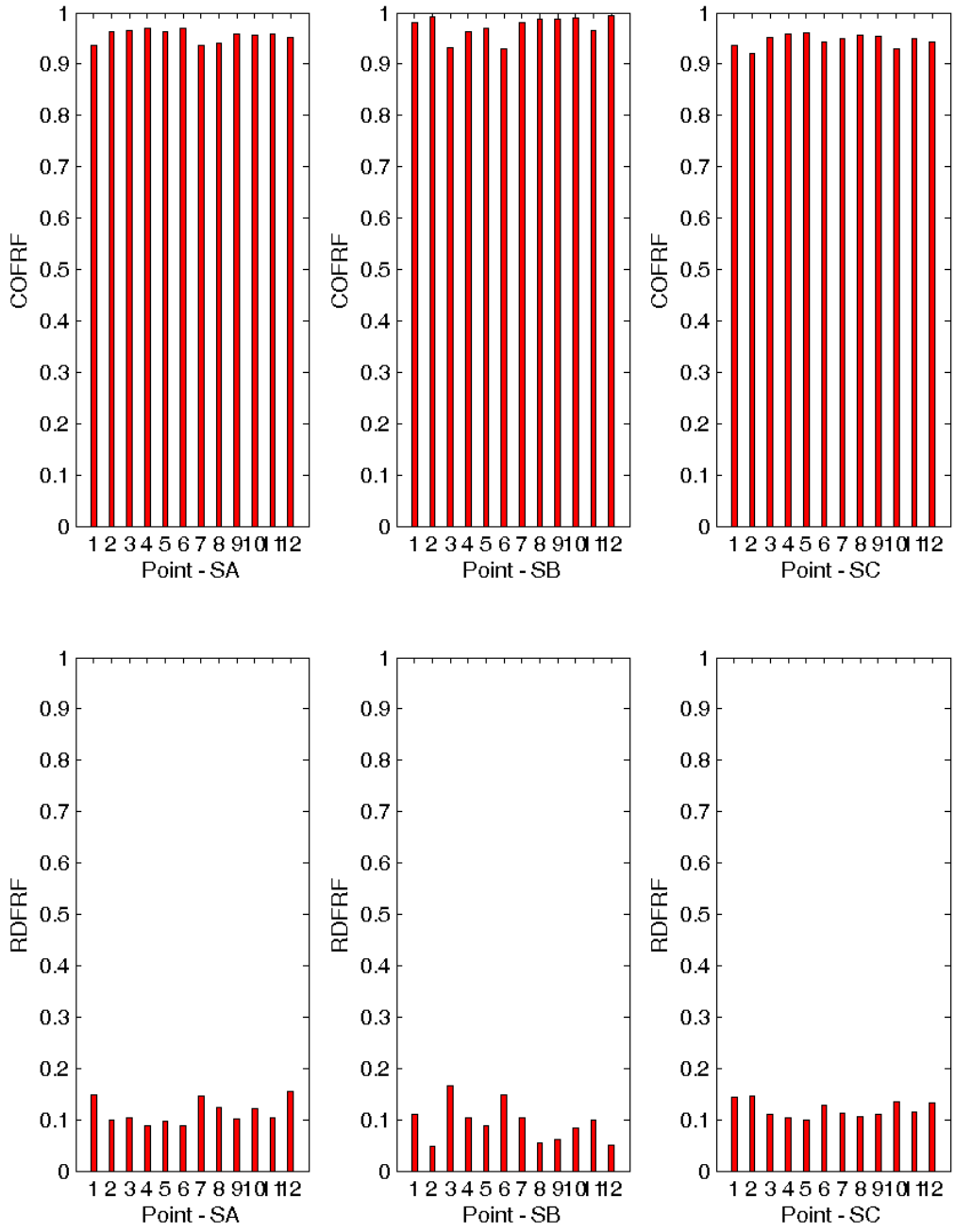

Figure 8. COFRF (upper) and RDFRF (bottom) between the slab and girders for undamaged state D0

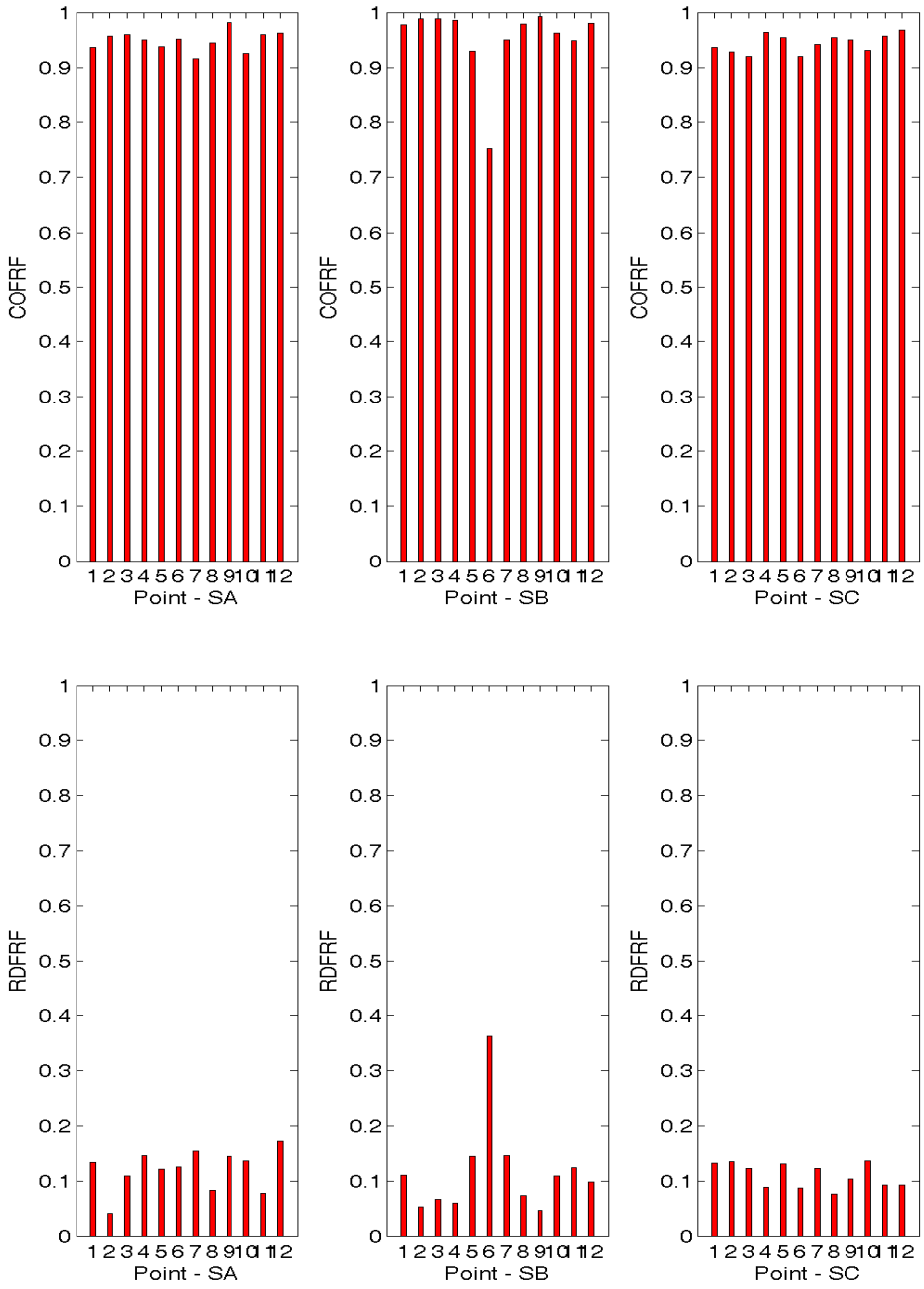

Figure 9. COFRF (upper) and RDFRF (bottom) between the slab and girders for the damaged state D1 (damage around SB6)

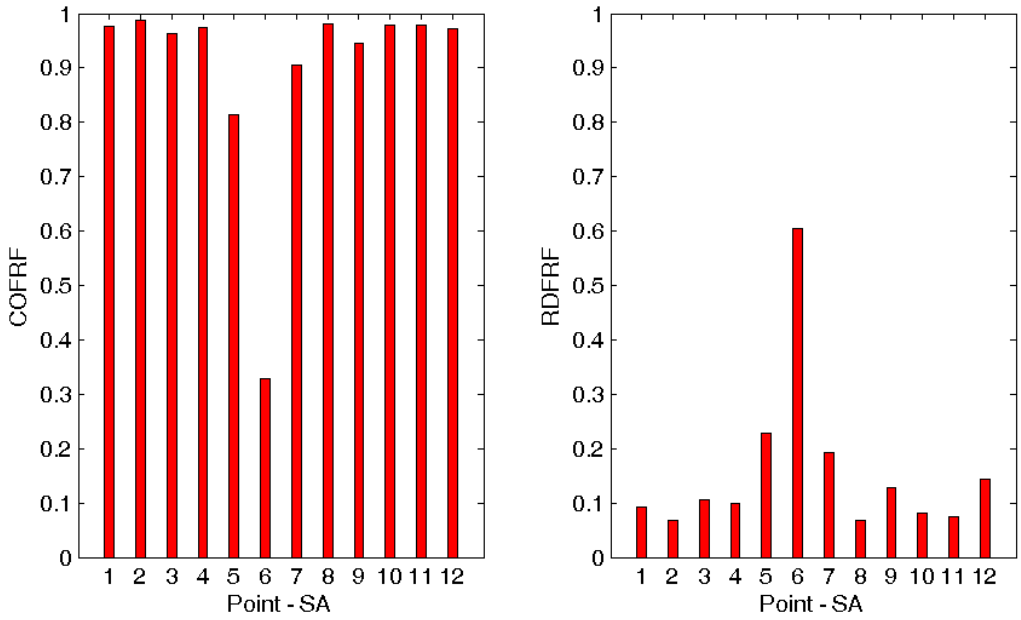

Figure 10. COFRF and RDFRF between the slab and Girder A for the damaged state D2 (damage around SA6)

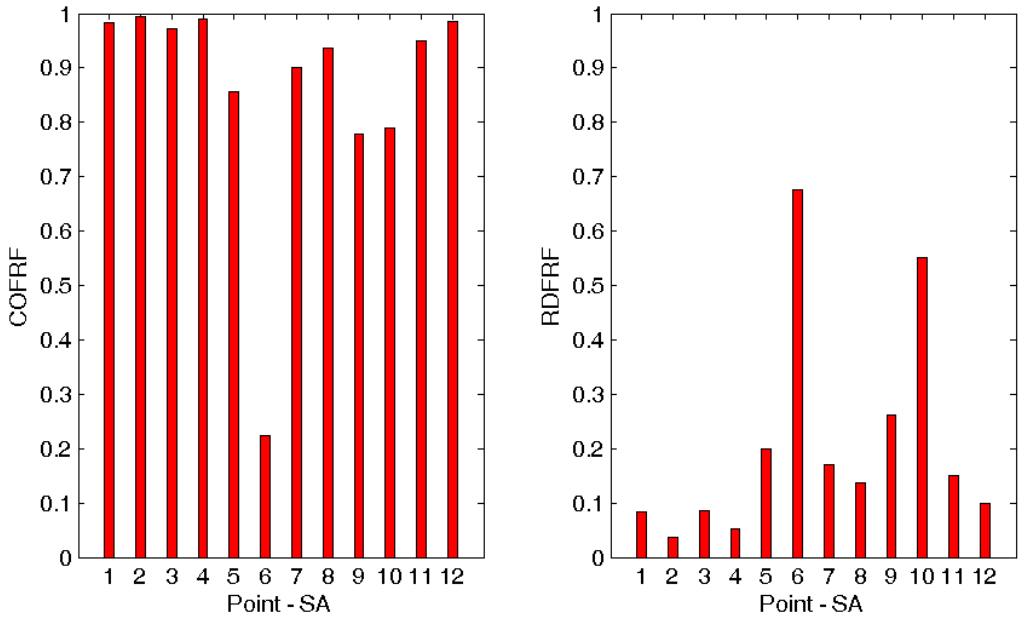

Figure 11. COFRF and RDFRF between the slab and Girder A for the damaged state D3 (damage around SA6 and SA10)

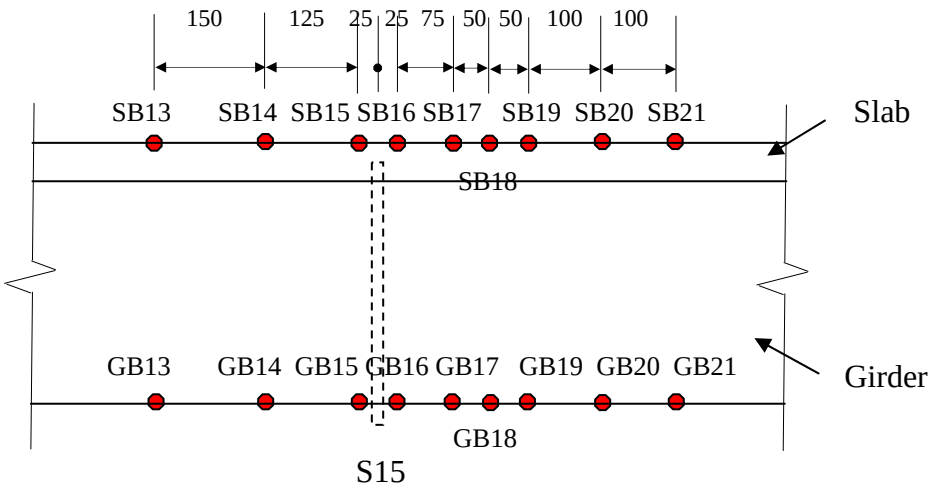

Figure 12. Sensor location around S15 (SB13~21 and GB13~21) to find the sensitive radius to damage (unit: mm)

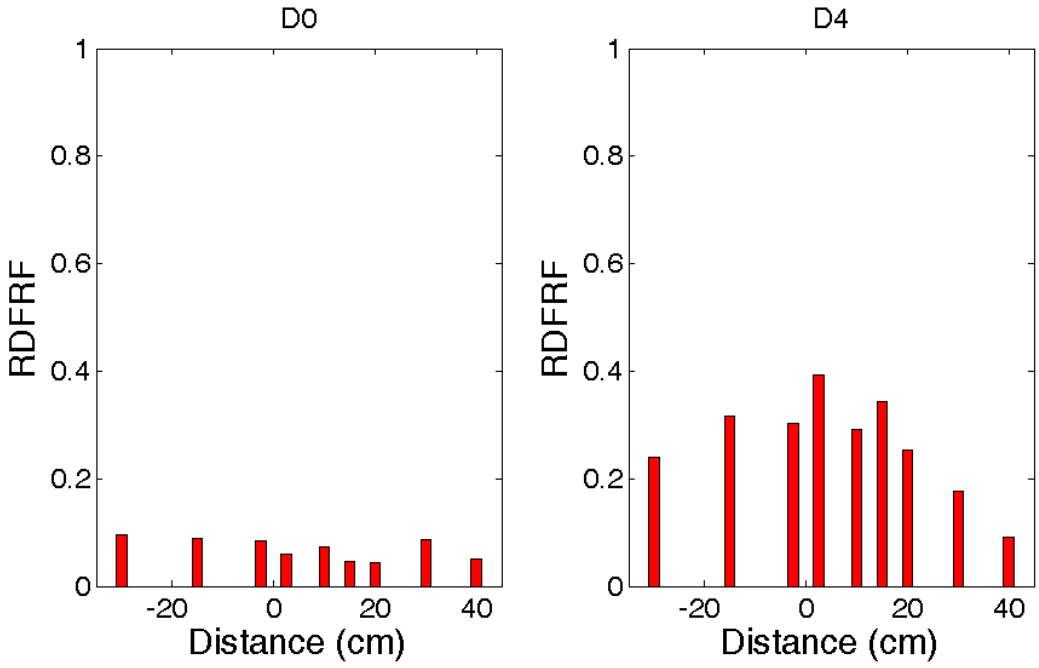

Figure 13. RDFRF for the damaged state D4 - testing

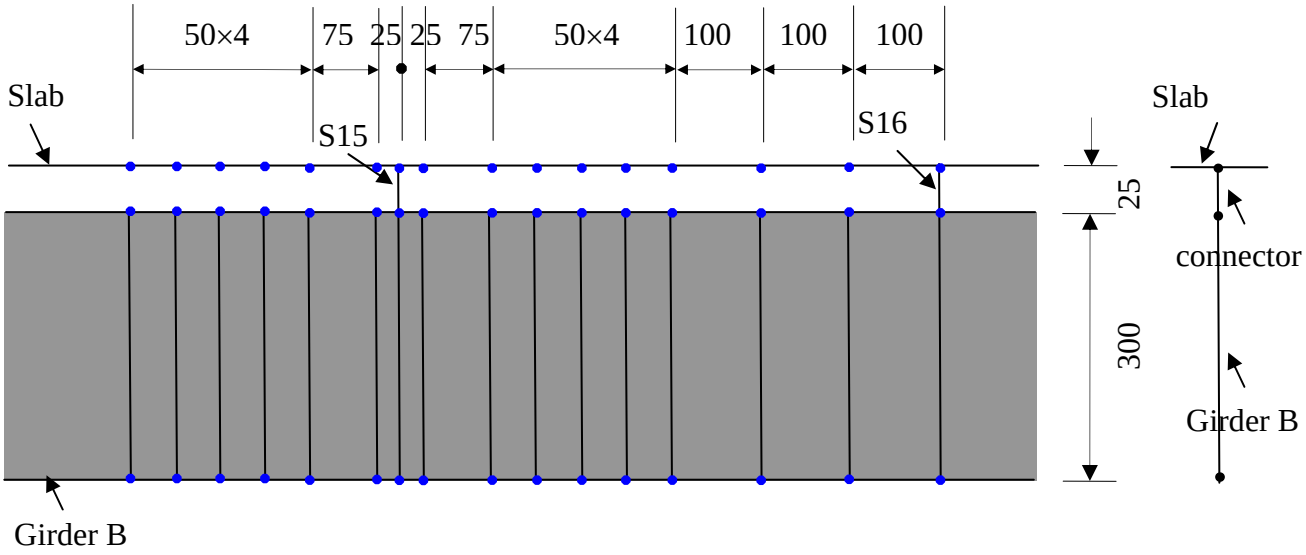

Figure 14. FE mesh in the slab and Girder B around S15 to determine the sensitive radius of damage (unit: mm). Left: elevation; right: section

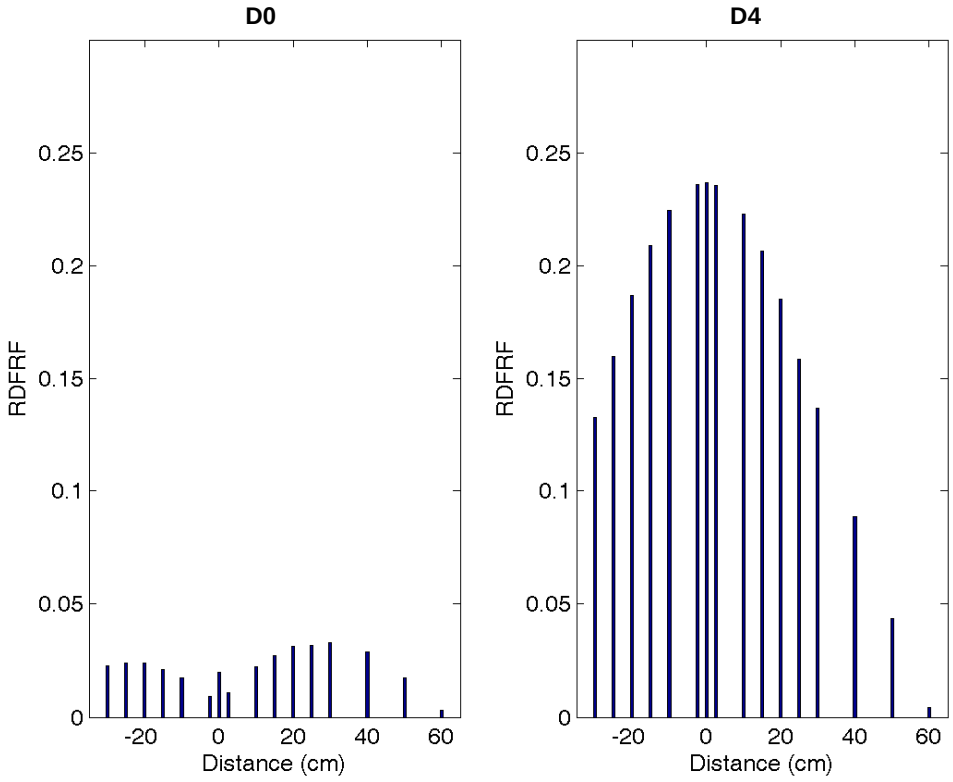

Figure 15. Relative difference of FRFs for D4 - FE simulation

Table 1. Measurement in each damage case

	Intact (D0)	D1 (S13 and S14 loosen)	D2 (S4 and S 5 loosen)	D3 (S4, 5, 8, 9 loosen)	D4 (S15 loosen)
On the slab	SA1~SA12 SB1~SB12 SC1~SC12	SA1~SA12 SB1~SB12 SC1~SC12	SA1~SA12 SB1~SB12 SC1~SC12	SA1~SA12 SB1~SB12 SC1~SC12	SB13~SB21*
Underneath the beams	GA1~GA12 GB1~GB12 GC1~GC12	GA1~GA12 GB1~GB12 GC1~GC12	GA1~GA12	GA1~GA12	GB13~GB21*

* Refer to Figure 12

Table 2**.** Comparison of modal data in D0 and D1

Mode	D0		D1		Difference (%) [+]	MAC [*]
	Frequency (Hz)	Damping ratio (%)	Frequency (Hz)	Damping ratio (%)		
1	16.70	0.87	16.67	0.90	-0.17	1.00
2	31.08	0.62	30.96	0.63	-0.38	1.00
3	57.26	1.11	56.54	1.03	-1.26	1.00
4	71.46	0.53	71.44	0.54	-0.03	1.00
5	84.63	0.57	83.60	0.65	-1.22	0.99
6	96.66	1.57	96.27	1.65	-0.40	1.00
7	116.91	1.09	114.79	0.98	-1.82	0.99
8	119.62	0.51	118.69	0.55	-0.78	0.97
9	123.54	0.22	123.37	0.24	-0.14	0.88
10	126.27	0.39	126.11	0.51	-0.13	0.99
11	129.70	0.50	128.44	0.70	-0.97	0.96
12	135.54	0.61	135.42	0.92	-0.09	0.88
13	141.28	1.20	136.39	1.08	-3.46	0.86
14	147.91	0.58	148.12	1.19	0.14	0.77
15	170.85	1.20	169.31	1.21	-0.90	0.96
16	173.72	0.68	173.70	0.73	-0.01	0.96
17	220.63	1.21	213.04	1.31	-3.44	0.79
18	224.04	0.35	219.16	1.01	-2.18	0.10
19	234.40	0.97	230.72	0.92	-1.57	0.78

[+] Relative difference of frequency between damaged and intact ones;
[*] Modal Assurance Criterion (MAC) of damaged mode shapes and intact ones